Improved Resolution for 3-D Position Sensitive CdZnTe Spectrometers

Feng Zhang, *Student Member, IEEE*, Zhong He, *Senior Member, IEEE*, Dan Xu, Glenn F. Knoll, *Fellow, IEEE*, David K. Wehe, *Senior Member, IEEE*, and James E. Berry

***Abstract*—Two three-dimensional position sensitive CdZnTe gamma-ray spectrometers based on VAS2/TAT2 ASICs were constructed and fully tested. Each $1.5 \times 1.5 \times 1$ cm^3 CdZnTe detector employs 11×11 pixelated anodes. Each pixel location provides the interaction's lateral coordinates, while the cathode/anode signal ratio and the electron drift time are both used to obtain the interaction depth. Data-acquisition and processing software were developed to perform calibration and real-time spectroscopy. An energy resolution of 1.11% full-width at half-maximum (FWHM) at 662 keV was obtained for single-pixel events from the 120 working pixels of one detector, and an energy resolution of 1.14% FWHM was obtained on the other detector. Significant progress in improving energy resolution for multiple pixel events has been realized. The energy resolutions at 662 keV for two-pixel events and three-pixel events were 1.57% FWHM and 2.13% FWHM, respectively.**

***Index Terms*—CdZnTe, CZT, gamma-ray spectroscopy, position sensitive, spectrometer, three-dimensional (3-D).**

I. Introduction

WIDE band gap semiconductor materials such as HgI_2, CdTe and CdZnTe have long been of interest for gamma-ray spectroscopy at room temperatures. However, severe charge trapping has limited their application when large sensitive volumes are needed. A single polarity charge sensing technique, e.g., a coplanar [1] or pixelated anode [2], successfully minimizes the hole-trapping problem and greatly improves the energy resolution for larger volume detectors. However, problems with material nonuniformity and spatially varying electron trapping still exist and limit the energy resolution. In 1998, the first fully functional 3-D CZT spectrometer was tested [3], [4]. The three-dimensional (3-D) position sensitivity of this CZT spectrometer using VA1 ASIC chips enabled the correction for material nonuniformity and varying electron trapping. An energy resolution of 1.7% full-width at half-maximum (FWHM) at 662 keV was achieved for single-pixel events from the whole bulk of a 1 cm^3 3-D CZT detector [3]. However, high electronic noise from dc-coupling limited the performance of these devices. The cathode signal had to be read out through discrete circuits and the relatively noisy grid signal had to be used as the system trigger. These devices were also incapable of correctly reading out the information for multiple-pixel events [4]. The simulation results showed that two-pixel events and three-pixel events constitute nearly 60% of the photopeak events at 662 keV, and multiple-pixel events are even more dominant at higher gamma-ray energies.

To eliminate the limitations of these first generation spectrometers, a second-generation of 3-D CZT spectrometers have been designed and fabricated using the Ideas ASA[1] VAS2/TAT2 ASIC chipsets. Peak-hold circuits, triggering circuits with mask, time sensing capability and AC-coupling equivalent circuits are significant enhancements included in the VAS2/TAT2 chipsets.

A comprehensive software platform has been developed to test the system, to carry out data acquisition, and to process the data. Most of the calibration procedures can be completed automatically by the software. The final calibration data is fed back to the data acquisition program to allow it to function as a real-time 3-D CZT spectrometer with COMPTON imaging capability [5].

This paper briefly introduces the basic system structure and the major calibration procedures. The experimental results from two separate detector systems using this system are presented.

II. System Description

The electronic readout system is based on the VAS2/TAT2 ASIC chipsets. The VAS2 (Voltage ASIC with Stretcher, version 2) channels are used to read out the induced charges on the anode pixels. The TAT2 (Trigger ASIC with Timing, version 2) channels are used to trigger the system and read out the electron drift times. One VAS2 chip and one TAT2 chip form a chipset. The preamplifier output of each VAS2 channel is wire-bonded to the input of each TAT2 channel. Four chipsets are needed for each 121-pixel CZT detector.

A. ASIC Structure

Each VAS2 chip has 32 independent channels, each consisting of a preamplifier, a 1-μs-shaping-time shaping amplifier and a peak-hold and sample-hold circuit. The first channel on each VAS2 chip has an opposite polarity to the other 31 channels, to read out the signal from the cathode. Fig. 1 shows the basic structure of a single VAS2/TAT2 channel.

Each TAT2 chip also has 32 channels, each channel having a 75-ns-shaping-time fast shaper, a discriminator for triggering and a TAC for electron drift time sensing. A trigger mask can be set to disable those channels having high noise.

Manuscript received November 15, 2003; revised May 25, 2004. This work was supported by the Department of Energy/NNSA NA-22 office under Grant DE-FG03-01NN20122.

The authors are with the Department of Nuclear Engineering and Radiological Sciences, University of Michigan, Ann Arbor, MI 48109 USA (e-mail: zhangf@umich.edu).

Digital Object Identifier 10.1109/TNS.2004.835635

[1]Ideas ASA, Martin Linges vei 25, Snarøya, Norway.

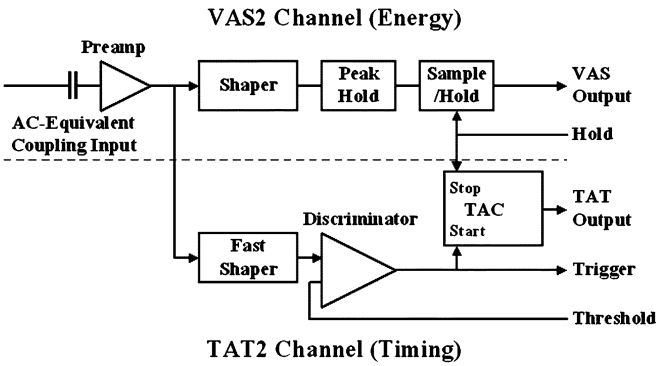

Fig. 1. Illustration for the VAS2 (energy) and the TAT2 (timing) channels.

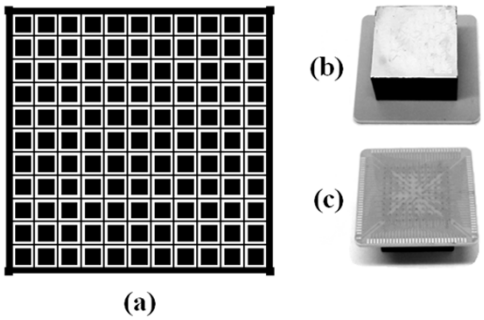

Fig. 2. (a). 11×11 anode pixel-grid pattern. (b). Photo of the detector with the cathode facing up. (c). Photo of the detector with the ceramic substrate facing up.

B. System Structure

The detector has an 11×11 pixelated anode and a single cathode on a $1.5 \times 1.5 \times 1.0$ cm^3 CZT crystal fabricated by eV-PRODUCTS.[2] The pixel pitch is 1.27 mm. There is a common grid between pixel anodes biased at negative voltage to focus the electrons to the pixel anodes. The trace width of the grid electrode is 100 μm with a 200 μm gap between the grid and the pixel. The anode pixel-grid pattern and the pictures of the detector are shown in Fig. 2(a)–(c).

Four VAS2/TAT2 chipsets are mounted on the front-end board to read out signals from 121 anode pixels and the cathode. The CZT crystal is mounted on a ceramic plate [cf. Fig. 2(b)]. The conducting traces within the multi-layer ceramic plate connect every pixel anode to a corresponding metal pad on the periphery of the plate [cf. Fig. 2(c)]. A short wire-bond connects each pad on the ceramic plate to the input of each ASIC channel on the front-end board. A controller and repeater card (MCR3) is used to generate and send the readout clock signals to the ASIC and also convert the output of the ASIC to the voltage signal needed at the input of the data acquisition (DAQ) board. A PCI-6110 DAQ board from National Instruments is used as the A/D converter and as the controller interface between the DAQ program and the detector system.

C. Depth Sensing Using Electron Drift Time

Fig. 3 summarizes the basic concept of depth sensing using electron drift time for multiple-pixel events. When a gamma-ray

[2]eV-PRODUCTS, 375 Saxonburg Boulevard, Saxonburg, PA 16065.

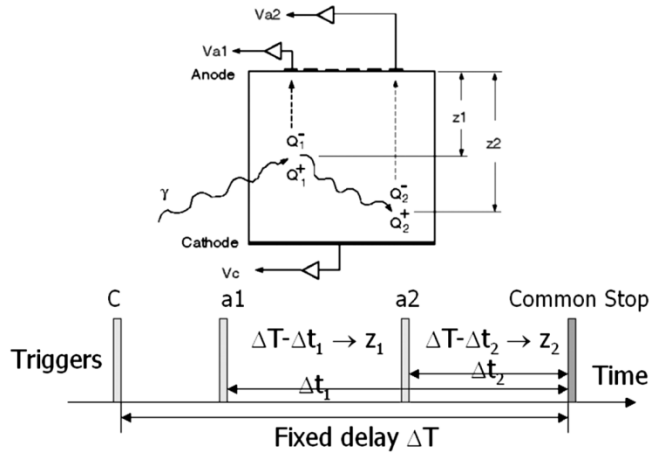

Fig. 3. Interaction depth determination by electron drift time sensing. Va1, Va2, and Vc are the signals from two anode pixels and the cathode, respectively.

interacts in the detector and the electron clouds start to drift, a trigger is generated by the TAT2 special channel when the induced signal on the cathode crosses a threshold. This trigger starts the TAC in the TAT2 special channel and generates the system trigger—C. When an electron cloud drifts near an anode pixel, the induced signal crosses a threshold, and triggers the corresponding TAT2 channel—a1. This trigger starts the TAC corresponding to that anode pixel channel. After a fixed delay ΔT after the system trigger, all the channels are read out in serial mode through a multiplexer built into the chips. By using peak-hold in addition to sample-hold circuits, the pulse amplitude of multiple-pixel events with different electron drift times (different peaking times) can be read correctly. The individual electron cloud drift times $(\Delta T - \Delta t_1, \Delta T - \Delta t_2, \ldots)$ can be retrieved from the timing signal generated by the TACs in the TAT2 channels.

D. Working Modes

The system can work in two readout modes: single-channel mode and serial readout mode. The single-channel mode is used for system testing. In this mode, the multiplexer is set so that one channel is constantly connected to the output and the test pulse generated by the DAQ board is injected into this channel. The output of this channel is read out continuously and the response of this channel, including voltage and timing response, to the test pulse can be monitored both in the DAQ program and on the oscilloscope. The serial read out mode is used to sequentially sample the output of all the channels by the multiplexer being automatically switched channel by channel by the readout clock. Sparse readout mode is not available so it requires $\sim$500 μs to read out the 128 channels. Thus, the throughput is limited to $\sim$2000 events per second.

E. Trigger and Threshold

Two trigger modes can be chosen in the serial readout mode, the program trigger or the TA-trigger. The program trigger is generated by a general-purpose counter on the DAQ board. The system can be read out at a constant rate by programming the general-purpose counter. The TA-trigger is generated by the TAT2 chip. The discriminator outputs from the TAT2 channels

are combined using "OR" logic to produce the TA-trigger. This is the mode used when serially reading events from the detector.

Ideally, the system should be triggered from the cathode side and the electron drift time could be derived from the time difference between the cathode trigger and the anode trigger. However, due to a layout design oversight, there is large cross-talk on the cathode signal induced by the digital clock signals. A special add-on circuit was integrated into the system to reduce the cross-talk and suppress the induced triggering with this alteration. The cathode signal lowest threshold is limited to 110 keV by cross-talk induced triggering. The anode pixels have triggering thresholds ranging from 60 to 90 keV, with the spread caused by the variation of baseline levels and noise in each ASIC channel. For single-pixel events, the system can be triggered from either the cathode side or the anode side because the cathode to anode signal ratio (C/A ratio) can be used for depth sensing [6]. For multiple-pixel events, the system has to be triggered from the cathode side. Each anode signal must also pass its threshold to register the electron drift time for its electron cloud. Since the cathode trigger signal is determined by the total energy deposition, while the anode trigger signals are determined by the smaller individual energy depositions, the system threshold for multiple-pixel events is mainly limited by the anode threshold lower limit.

In the current system, only a global threshold can be set for all the anode pixels. Thus, the global threshold has to be set above the highest threshold among all channels to avoid noise triggering. In our next design, a DAC threshold for each channel should allow more uniform thresholds for all channels and a lower global threshold.

III. Calibrations

Due to the nonuniformity in both the detector material and the electronics, various calibrations are necessary to achieve good energy resolution. A data processing program has been developed using C++, and most of the calibrations can be done automatically.

A. Baseline Drift and Gain Drift Correction

Unlike the VA1 chips, the channels on the VAS2 chips have significant baseline sensitivity to temperature changes. The baseline drift can be monitored in real time and subtracted during the data acquisition. The gain drift was found to have a monotonic relation with the VAS2 output baseline position, as shown in Fig. 4. Thus, the gain variation can be corrected by monitoring the baseline shift in real time and using this relationship.

B. Depth Correction Using C/A Ratio and Electron Drift Time

For single-pixel events, the ratio of the cathode signal and the anode signal can be used to get the interaction depth [6]. This depth information can be used to sort the events into spectra for different depths. Then, the spectra from all the depths can be combined by aligning the 662 keV photopeak to the same position [7]. As a result, the material nonuniformity and the variations in electron trapping and weighting potential are corrected down to the limit of the position resolution over the whole detector volume.

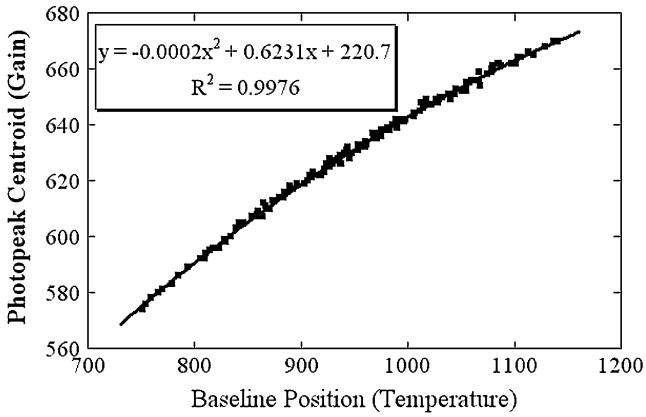

Fig. 4. Correlation of photopeak position (gain) versus baseline position (temperature) over a 40-h measurement. The temperature range is 21 °C–26 °C.

However, for multiple-site events, the individual depths for each interaction site cannot be derived from the cathode/anode signal ratio. In our second-generation 3-D CZT spectrometers, the electron drift time is used to determine the depth of each interaction site. Using the cathode trigger generated when the electron clouds start to move, a fixed delay added to this as the common stop, and the pixel trigger when the electron cloud approaches the anode as the start for that pixel, the electron drift time can be digitized and read out for each pixel.

For single-pixel events, either the C/A ratio or the electron drift time can be used to get the interaction depth and to derive the depth correction coefficients. However, due to limited timing resolution (∼30–40 ns), the depth correction coefficients derived from the electron drift time are worse than those derived from the C/A ratio depth, and, consequently, result in poorer energy resolution. So, only the C/A ratio and the depth correction coefficients derived from the C/A ratio are used for single-pixel events.

For multiple-pixel events, although we can only get the interaction depth from the electron drift time, we still want to use the better depth correction coefficients derived from the C/A ratio in the single-pixel events calibration. Thus, the relation between the C/A ratio and the electron drift time must first be calibrated for single-pixel events, as shown in Fig. 5. Then, for multiple-pixel events, the equivalent C/A ratio can be deduced from the electron drift time for each pixel. As a result, mapping the electron drift time to the C/A ratio and using the depth correction coefficients derived from the C/A ratio result in better energy resolution than only using the electron drift time.

C. Nonlinearity Correction

Although the dynamic range of the VAS2 channels accommodates energy deposition up to 1 MeV, the VAS2 channels have significant nonlinearity even at 662 keV (8% deficit from the linear relation). Thus, an energy calibration using multiple energy sources must be carried out. For multiple-pixel events, because the total deposited energy has to be derived from the sum of the deposited energy by each individual interaction, an

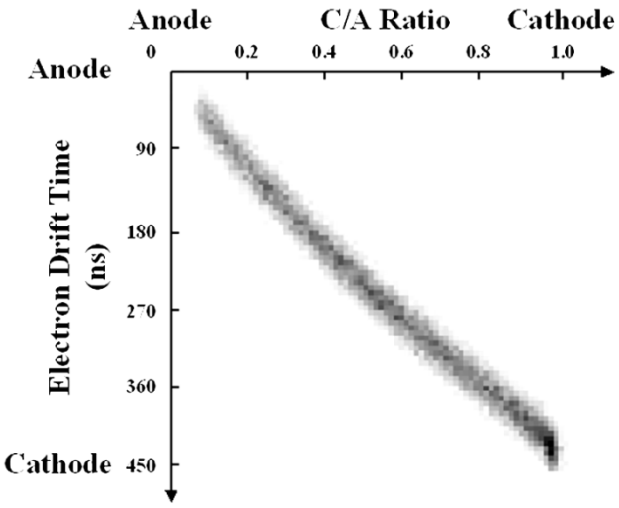

Fig. 5. Correlation between C/A ratio and electron drift time.

accurate energy calibration is especially important for good energy resolution. By implementing the nonlinearity calibration, the energy resolution for two-pixel events improved from $>5\%$ to $<2\%$ for 662 keV.

D. Timing Amplitude-Walk Correction

Timing amplitude-walk was observed for both anode and cathode timing signals in the VAS2/TAT2 system. To get the true electron drift time for multiple-pixel events over the whole energy range, a timing calibration was performed for all channels.

IV. Experimental Results

Two detectors of identical dimensions were tested. The cathode bias voltage was chosen for the stability of the cathode signal. The grid bias voltage was based on an electric field calculation to prevent charge sharing on the grid electrodes. The first detector was biased at -2200 V on the cathode and -85 V on the anode grid. The second detector was biased at -2000 V on the cathode and -80 V on the anode grid. The anode pixels were at ground potential and connected to the input of the ASIC by wire-bonds. Both detectors were irradiated from the cathode side with gamma-ray sources placed 5 cm away from the cathode. The ^{137}Cs 662 keV gamma-ray spectra shown below were acquired over 40 h for each detector. Spectra from ^{133}Ba, ^{57}Co and ^{22}Na gamma-ray sources were also collected for the nonlinearity calibration.

After the corrections, the energy resolution (FWHM) for single-pixel events is shown in Fig. 6 for both detectors. The overall resolutions (FWHM) for events from the whole volume of each detector are shown in Table I.

From Fig. 6, we can see that the first detector has better overall material quality than the second detector. One reason for the second detector's worse performance is the material or surface defects shown in the top three rows. The ASIC chip used to read out signals from that region also has a smaller gain and worse signal/noise ratio than the ASICs used to read out other regions. However, in the good regions of the second detector, there are more pixels that have an energy resolution of better than 1%. The overall energy resolution of the second detector is similar to that of the first detector, as can be seen in Table I.

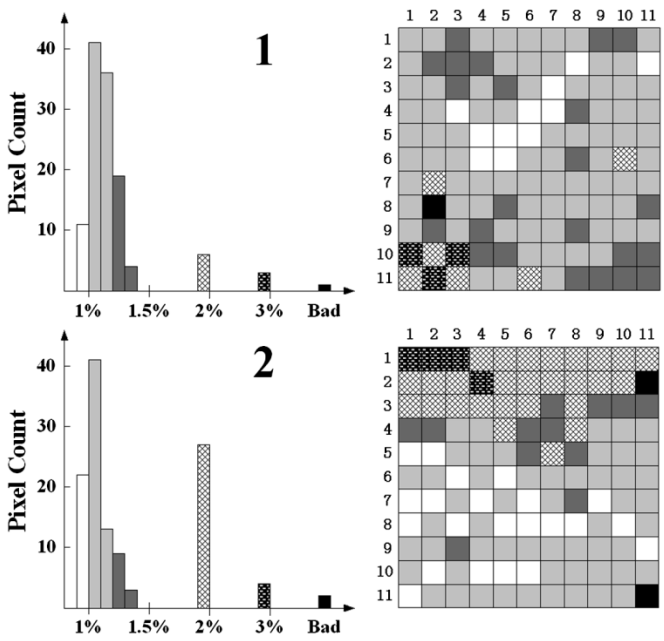

Fig. 6. Energy resolution distribution for single-pixel events from a ^{137}Cs source collected over 40 h for (1). Detector 1. (2). Detector 2.

TABLE I
Energy Resolution (FWHM) at 662 keV for Single-Pixel Events and Multiple-Pixel Events From the Whole Bulk of Two Similar Detectors

Detector	Single-Pixel Events	Two-Pixel Events	Three-Pixel Events	Four-Pixel Events
1 @ -2200 V, -85 V	1.11% (7.3 keV)	1.57% (10.4 keV)	2.13% (14.1 keV)	2.64% (17.5 keV)
2 @ -2000 V, -80 V	1.14% (7.5 keV)	1.64% (10.9 keV)	2.28% (15.1 keV)	2.81% (18.6 keV)

The overall spectra for single-pixel events, two-pixel events and three-pixel events from the whole first detector are shown in Fig. 7. The rather complete absorption of the gamma-ray for multiple-pixel events is evident from the lack of background counts in Fig. 7(b) and (c), and is one important feature of the intelligent gamma-ray spectroscopy [8].

Before the detector is wire-bonded to the ASIC, the electronic noise can be measured by directly injecting a test pulse into the input pads of the ASIC. However, this is impossible to do without damaging the wire-bonds after the detector has been wire-bonded to the ASIC and the bias voltage applied to the detector. Due to this limitation, the electronic noise cannot be measured directly. Instead, the energy resolution measured for a low-energy gamma-ray was used to estimate the electronic noise. Because of the high system threshold discussed above, 60-keV photons from ^{241}Am cannot be observed. Instead, a ^{133}Ba gamma-ray source was used to irradiate the detector from the cathode side. Most of the 81 keV photoelectric events should take place in a thin layer near the cathode. The FWHM of the 81-keV photopeak was then used to estimate the electronic noise of the system and found to be $\sim$6 keV FWHM.

Theoretically, given the estimated electronic noise of 6-keV FWHM on the anode signal and 9-keV FWHM on the cathode signal, a depth resolution of $\sim$0.15 mm should be achievable on a 1 cm thick CdZnTe detector using C/A ratio at 662-keV

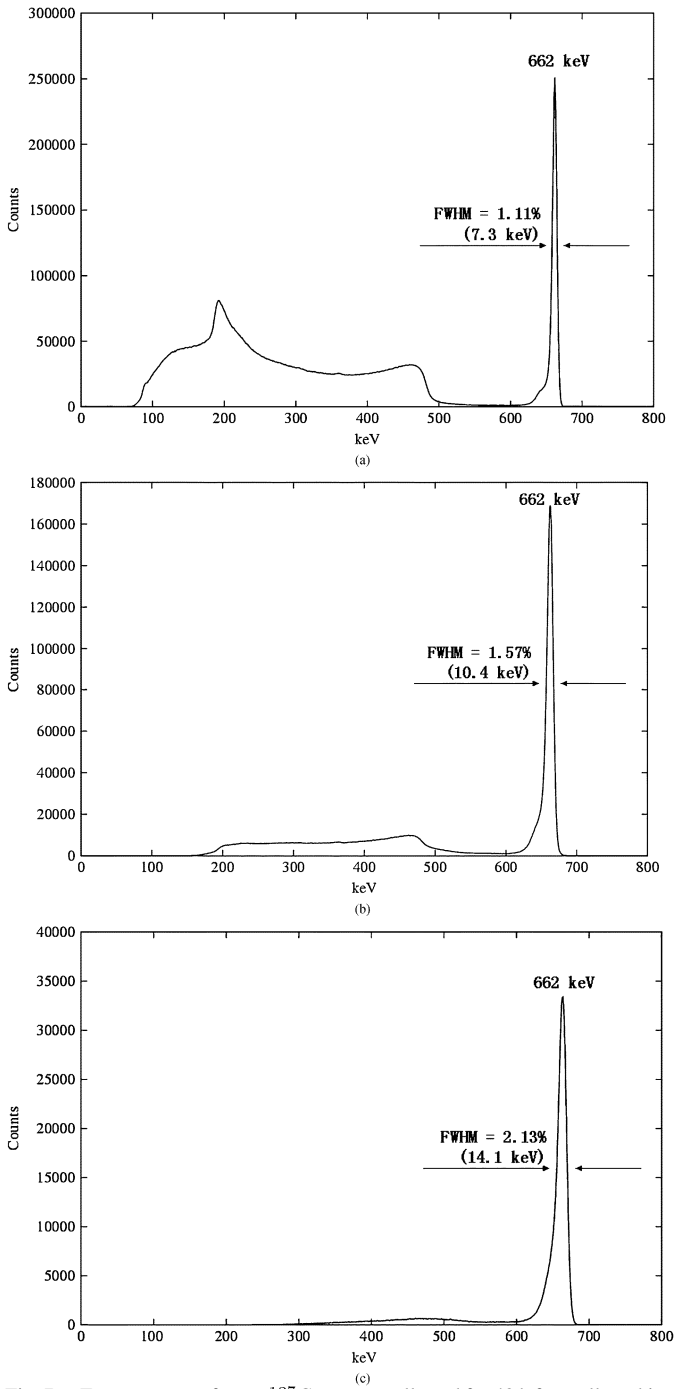

Fig. 7. Energy spectra from a ^{137}Cs source collected for 40 h from all working pixels in detector 1. (a) Single-pixel events. (b) Two-pixel events. (c) Three-pixel events.

gamma-ray energy [9]. Experimentally, the depth resolution using C/A ratio was estimated to be ∼0.25 mm because dividing the depths into more than 40 bins cannot further improve the energy resolution. However, the depth resolution using electron drift time has been estimated to be ∼0.8 mm due to the poor (∼30–40 ns) timing resolution. This is one of the major reasons for the degradation of energy resolution from 1.11% for single-pixel events to 1.57% for two-pixel events at 662 keV. Added electronic noise from multiple pixels, nonoptimized correction of gain drift, and gain nonlinearity may further degrade the energy resolution for multiple-pixel events.

V. Summary and Conclusion

Two $1.5 \times 1.5 \times 1.0$ cm^3 CdZnTe detectors, each with 11×11 pixelated anodes were fabricated by eV-Products. The signals from the 121 anode pixels and the cathode were read out by four pairs of 32 channel VAS2/TAT2 ASICs. One detector was tested with −2200 V cathode bias and −85 V anode-grid bias, and the other with −2000 V cathode bias and −80 V anode-grid bias. Gamma-ray events from ^{137}Cs 662 keV were collected and analyzed. Baseline shift, gain variation and nonlinearity were individually calibrated for each channel automatically in software. Material nonuniformity and electron trapping corrections were calibrated based on the 3-D position of interaction. Corrections for nonuniform electron transport are essential for all events, and corrections for ASIC gain nonlinearity were important for multiple-pixel events.

The basic principle of the system and the major calibration procedures has been discussed in this paper. A software platform has been developed to complete most of the data acquisition and calibration procedures automatically, making the system easy to operate.

Energy spectra for single-, two-, and three-pixel events from the 120 working anode pixels of one detector at 662 keV were 1.11% (7.3 keV), 1.57% (10.4 keV) and 2.13% (14.1 keV), respectively. Similar performance was observed on an identical second detector. Limiting factors for the energy resolution of multiple pixel events include added electronic noise and depth resolution from the electron drift time.

Acknowledgment

The authors would like to thank A. B. Young of the Radiation Oncology Department and B. E. Casey of the Electrical Engineering and Computer Science Department, the University of Michigan, for their work on wire bonds.

References

[1] P. N. Luke, "Unipolar charge sensing with coplanar electrodes-application to semiconductor detectors," *IEEE Trans. Nucl. Sci.*, vol. 42, pp. 207–213, Aug. 1995.

[2] F. P. Doty, H. B. Barber, F. L. Augustine, J. F. Butler, B. A. Apotovsky, E. T. Young, and W. Hamilton, "Pixelated CdZnTe detector arrays," *Nucl. Instrum. Meth. A*, vol. 353, pp. 356–360, 1994.

[3] Z. He, W. Li, G. F. Knoll, D. K. Wehe, J. E. Berry, and C. M. Stahle, "3-D position sensitive CdZnTe gamma-ray spectrometers," *Nucl. Instrum. Meth. A*, vol. 422, pp. 173–178, 1999.

[4] W. Li, Z. He, G. F. Knoll, D. K. Wehe, and J. E. Berry, "A data acquisition and processing system for 3-D position sensitive CZT gamma-ray spectrometers," *IEEE Trans. Nucl. Sci.*, vol. 46, pp. 1989–1994, Dec. 1999.

[5] C. E. Lehner, Z. He, and F. Zhang, "4 π compton imaging using a 3-D position-sensitive CdZnTe detector via weighted list-mode maximum likelihood," *IEEE Trans. Nucl. Sci.*, to be published.

[6] W. Li, Z. He, G. F. Knoll, D. K. Wehe, and Y. F. Du, "A modeling method to calibrate the interaction depth in 3-D position sensitive CdZnTe gamma-ray spectrometers," *IEEE Trans. Nucl. Sci.*, vol. 47, pp. 890–894, June 2000.

[7] W. Li, Z. He, G. F. Knoll, D. K. Wehe, and C. M. Stahle, "Spatial variation of energy resolution in 3-D position sensitive CZT gamma-ray spectrometers," *IEEE Trans. Nucl. Sci.*, vol. 46, pp. 187–192, June 1999.

[8] C. E. Lehner, Z. He, and G. F. Knoll, "Intelligent gamma-ray spectroscopy using 3-D position-sensitive detectors," *IEEE Trans. Nucl. Sci.*, vol. 50, pp. 1090–1097, Aug. 2003.

[9] Z. He, G. F. Knoll, D. K. Wehe, and J. Miyamoto, "Position-sensitive single carrier CdZnTe detectors," *Nucl. Instrum. Meth. A*, vol. 388, pp. 180–185, 1997.